

Disordered collective motion in dense assemblies of persistent particles

Yann-Edwin Keta,¹ Robert L. Jack,^{2,3} and Ludovic Berthier^{1,2}

¹*Laboratoire Charles Coulomb (L2C), Université de Montpellier, CNRS, 34095 Montpellier, France*

²*Yusuf Hamied Department of Chemistry, University of Cambridge, Lensfield Road, Cambridge CB2 1EW, United Kingdom*

³*Department of Applied Mathematics and Theoretical Physics, University of Cambridge, Wilberforce Road, Cambridge CB3 0WA, United Kingdom*

(Dated: January 14, 2022)

We simulate a two-dimensional model of size polydisperse self-propelled particles to explore the emergence of nonequilibrium collective motion in disordered non-thermal active matter when persistent motion and crowding effects compete. In stark contrast with monodisperse systems, we find that polydispersity stabilizes a homogeneous active liquid at arbitrary large persistence length, characterized by remarkable velocity correlations and irregular turbulent flows. For all persistence values, the active fluid undergoes at large density a nonequilibrium glass transition accompanied by collective motion, whose nature evolves qualitatively from near-equilibrium spatially heterogeneous dynamics at small persistence to an intermittent dynamics leading to a non-trivial time evolution of the correlated displacement field at large persistence.

Active matter constitutes a prominent class of nonequilibrium systems [1]. Examples in biological systems range from tissues [2] to bird flocks [3] and human crowds [4]. Synthetic active systems include robot swarms [5] and self-catalytic colloids, which have inspired numerous theoretical studies. In particular, self-propelled particles are paradigmatic theoretical models for active matter, where the variation of a few parameters leads to rich collective behaviour [6].

This work focusses on the interplay of motility and crowding in such models, which is relevant in both synthetic [7] and living systems [2]. It is well-known that persistent motility can trigger phase separation (MIPS) [8]; it also leads to nonequilibrium velocity correlations [9], possibly connected to active turbulence [10]. A different set of phenomena are associated with crowding effects in systems with modest persistence lengths: they undergo nonequilibrium glass transitions at high density [11, 12]. This transition shares many features with its equilibrium counterpart [13], such as two-step relaxation dynamics and slow, spatially correlated motion. It has been thoroughly studied using theory [14–16], simulations [11, 17–19], and experiments [7, 20].

In the following we present numerical simulations that unify this active glass phenomenology with the effects of crowding at much larger persistence lengths, where recent exploratory works have suggested the emergence of intermittent plasticity [10], analogies to yielding transitions [21–23], and a breakdown of equipartition in the disordered solid [24, 25]. We intentionally use active particles with size polydispersity, to ensure the stability of disordered states in crowded systems. Hence, our results (for example Fig. 1) parallel the similar programme that was recently completed for monodisperse particles, which display ordered phases at large density [26–28].

We find that polydispersity stabilizes a homogeneous liquid at large persistence [29, 30], characterised by cor-

related displacement fields. Moreover, on increasing the density of this active liquid, its behaviour differs strongly from the usual active glass transition [11, 12]. The approach to dynamical arrest is accompanied by an inherently active form of spatially heterogeneous dynamics, distinct from the phenomenology of passive glasses.

We simulate N athermal self-propelled particles in a square box of linear size L with periodic boundary conditions, with overdamped dynamics:

$$\xi \dot{\mathbf{r}}_i = - \sum_{j \neq i} \nabla_i U(r_{ij}) + \mathbf{p}_i, \quad (1)$$

where \mathbf{r}_i is the position of particle i , $r_{ij} = |\mathbf{r}_i - \mathbf{r}_j|$, ξ a viscous damping, and \mathbf{p}_i a persistent propulsion force. Particles interact via a repulsive Weeks-Chandler-Andersen potential $U = 4\epsilon [(\sigma_{ij}/r_{ij})^{12} - (\sigma_{ij}/r_{ij})^6 + 1/4] \Theta(2^{1/6}\sigma_{ij} - r_{ij})$, where Θ is the Heaviside function, $\sigma_{ij} = \frac{1}{2}(\sigma_i + \sigma_j)$, and σ_i is the diameter of particle i . Diameters are drawn from a

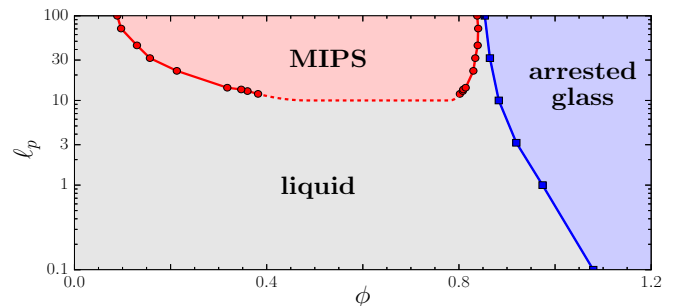


FIG. 1. Disordered active states when packing fraction and persistence length are varied at constant $D_0 = 1$. The MIPS region corresponds to phase separation. The homogeneous active liquid displays various types of collective motion when the persistence length is increased and/or the packing fraction is increased towards the nonequilibrium glass transition.

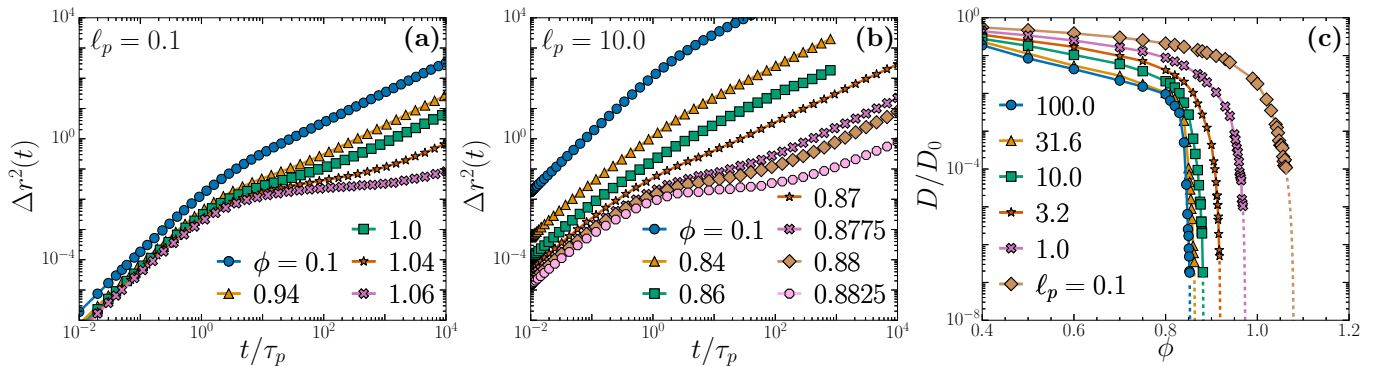


FIG. 2. (a, b) Mean squared displacements for different packing fractions ϕ , at persistence length (a) $\ell_p = 0.1$ and (b) $\ell_p = 10$, for $N = 1024$. (c) Density evolution of the scaled diffusion constant D/D_0 for different persistence lengths ℓ_p , for $N = 1024$. Dashed lines correspond to algebraic fits.

uniform distribution of mean $\sigma = \bar{\sigma}_i$ and polydispersity 20%. The packing fraction is $\phi = 2^{1/3} \pi N \bar{\sigma}_i^2 / (4L^2)$, σ sets the unit length, ε the unit energy, and $\xi \sigma^2 / \varepsilon$ the unit time. We measure the positions \mathbf{r}_i and velocities \mathbf{v}_i in the center-of-mass frame, such that $\sum_i \mathbf{v}_i = 0$.

Different self-propulsion models differ by the dynamics of \mathbf{p}_i . For active Brownian and run-and-tumble particles [31], $|\mathbf{p}_i|$ is fixed. We consider active Ornstein-Uhlenbeck particles [32, 33]:

$$\tau_p \dot{\mathbf{p}}_i = -\mathbf{p}_i + \sqrt{2D_0} \boldsymbol{\eta}_i, \quad (2)$$

with $\boldsymbol{\eta}_i$ a Gaussian white noise of zero mean and variance $\langle \boldsymbol{\eta}_i(t) \boldsymbol{\eta}_j(0) \rangle = \mathbb{1} \delta_{ij} \delta(t)$, and τ_p the persistence time. The amplitude and correlation time of \mathbf{p}_i can be varied independently so there are three control parameters (ϕ, D_0, τ_p). The parameter space reduces to (ϕ, τ_p) for self-propelled hard disks [17], while adding a thermal noise in Eq. (1) would instead make the phase diagram four-dimensional [30]. From Eqs. (1, 2), we see that D_0 is the diffusion constant of a free particle, the typical amplitude of the propulsion is $\sqrt{\langle |\mathbf{p}_i|^2 \rangle} = \sqrt{2D_0 / \tau_p} \equiv v_0$, and the persistence length $\ell_p = \sqrt{D_0 \tau_p}$. When $\tau_p \rightarrow 0$, equilibrium Brownian dynamics at temperature $T_{\text{eff}} = D_0$ is recovered with the usual control parameters (ϕ, T_{eff}). We have numerically explored the full three-dimensional phase diagram of the model and found that its main features are understood by keeping D_0 constant and varying the persistence time τ_p (equivalently, the persistence length ℓ_p). We show results for $D_0 = 1$, so that equilibrium at $T_{\text{eff}} = 1$ is recovered when $\tau_p = 0$, but the system is out of equilibrium in the entire (ℓ_p, ϕ) phase diagram in Fig. 1. As $\tau_p \rightarrow \infty$, the interaction term in (1) dominates over propulsion and particles effectively become hard.

Figure 1 shows the three disordered phases of polydisperse self-propelled disks. The homogeneous fluid appears for intermediate packing fraction and persistence length $\ell_p \lesssim 10$; it phase separates in the MIPS region at larger persistence. The MIPS boundaries were established by locating the two peaks of the probability

distribution function of the local packing fraction [27]. We only sketch the critical point of MIPS, its precise characterisation requiring a more detailed analysis [34]. Unlike monodisperse particles, whose relaxation relies on the movement of defects [35], the dense phase of MIPS is fully disordered and flows easily: it corresponds to an active liquid phase which exists up to arbitrarily large persistence in between MIPS and dynamic arrest, see Fig. 1.

For all ℓ_p , the active liquid undergoes a dynamic arrest at large ϕ , where it transforms into an active glass [11]. To characterise the liquid-glass boundary, we analyse the mean-squared displacement (MSD)

$$\Delta r^2(t) = \frac{1}{N} \sum_i \langle |\mathbf{r}_i(t) - \mathbf{r}_i(0)|^2 \rangle, \quad (3)$$

where brackets indicate an ensemble average. Results are shown in Fig. 2. In the liquid, the MSD is ballistic at short times, $\Delta r^2 \sim (vt)^2$, and diffusive at long times, $\Delta r^2 \sim 4Dt$. These limits define the mean-squared velocity, $v^2(\phi) \equiv \langle |\mathbf{v}_i|^2 \rangle$, and the self-diffusion constant, $D(\phi)$, which respectively reduce to v_0^2 and D_0 in the dilute limit, $\phi \rightarrow 0$.

In Figs. 2(a,b), we contrast the ϕ -dependent MSDs at small and large ℓ_p . In both cases, $D(\phi)$ decreases by several orders of magnitude when ϕ varies over a modest range, see Fig. 2(c). As in equilibrium systems, the determination of a critical packing fraction for dynamic arrest is ambiguous [36]: we fit $D(\phi)$ to an algebraic form inspired by mode-coupling theory, $D \sim (\phi_c - \phi)^\gamma$, to estimate a liquid-glass boundary $\phi_c(\ell_p)$ in Fig. 1.

The MSD data in Figs. 2(a,b) both show the emergence at large ϕ of a two-step relaxation process separated by a subdiffusive plateau. However, despite these similarities, the remainder of this work demonstrates several important differences between the highly-persistent case and weakly persistent (or equilibrium) glasses.

In equilibrium systems, velocities are spatially uncorrelated and obey the Maxwell distribution. The resulting

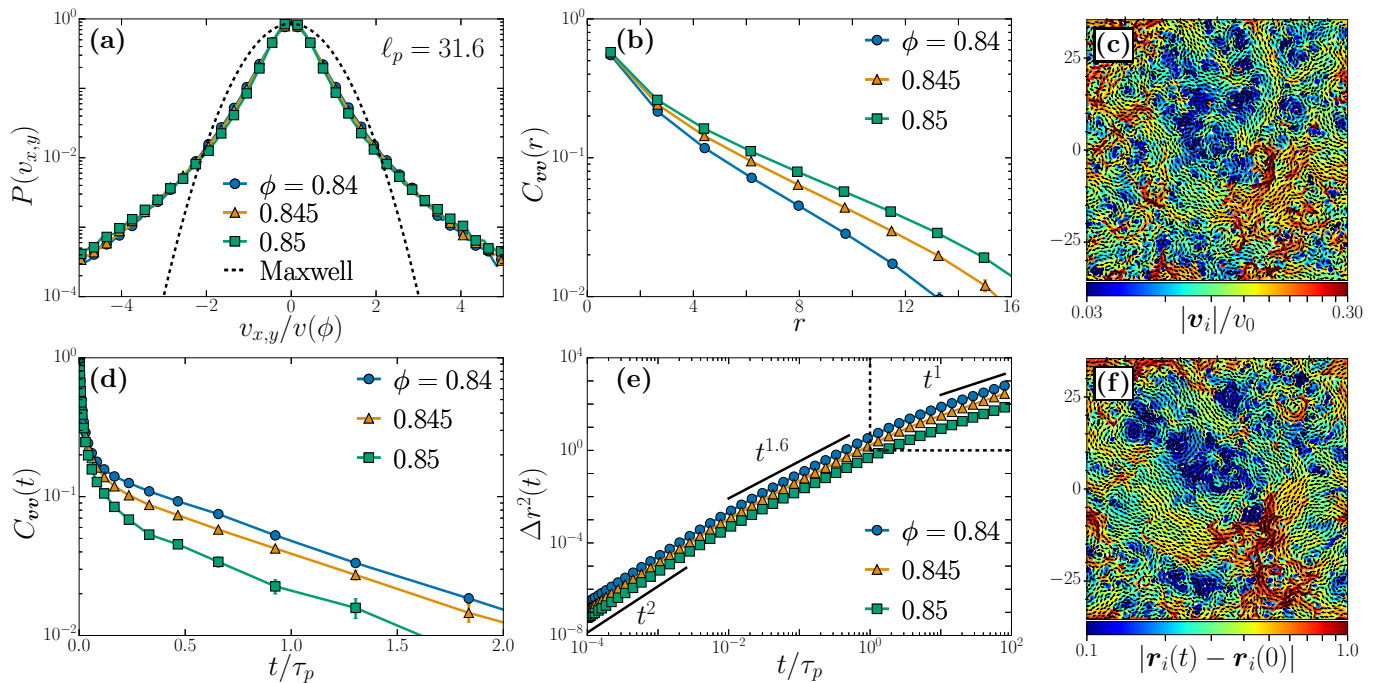


FIG. 3. (a) Velocity distribution $P(v_{x,y})$ for different packing fractions ϕ measured along the x and y directions. The dashed line corresponds to the Maxwell distribution. (b) Spatial correlations of the velocities $C_{vv}(r) = \langle \mathbf{v}_i(0) \cdot \mathbf{v}_j(0) \delta(r - r_{ij}) \rangle / v(\phi)^2 \langle \delta(r - r_{ij}) \rangle$ with $r_{ij} = |\mathbf{r}_i(0) - \mathbf{r}_j(0)|$. (c) Example of a velocity field for $N = 4096$, $\ell_p = 31.6$, $\phi = 0.84$. (d) Time autocorrelations of the velocity $C_{vv}(t) = \langle \mathbf{v}_i(t) \cdot \mathbf{v}_i(0) \rangle / v(\phi)^2$. (e) Mean-squared displacements for $\ell_p = 31.6$ and $N = 4096$ with ballistic, superdiffusive and diffusive behaviours indicated. (f) Displacement field after a time $t = 0.11\tau_p$ starting from the velocity field shown in (c) at $t = 0$.

mean-squared velocity v^2 is independent of ϕ and depends trivially on D_0 . The situation is very different in persistent systems, where $v^2(\phi)$ decreases sharply with ϕ , see Fig. 2(b). This already signals the importance of nonequilibrium effects on the velocities of interacting self-propelled particles [6, 25, 37].

In Fig. 3, we analyse particle dynamics in a highly persistent liquid whose density ϕ is between MIPS and dynamic arrest, at $\ell_p = 31.6$. As anticipated, the velocity distributions in Fig. 3(a) are strongly non-Maxwellian with much broader tails. Since a Gaussian distribution is expected both for interacting equilibrium particles and for non-interacting Ornstein-Uhlenbeck propulsions, the measured distributions reveal the non-trivial influence of many-body interactions in persistent liquids [25, 37].

Even more interestingly, persistent propulsions in the homogeneous liquid produce spatial velocity correlations [9, 18, 24, 38], which we quantify in Fig. 3(b) via the velocity correlation $C_{vv}(r)$ [39]. The data clearly reveal the existence of correlations extending over a lengthscale which grows with ϕ and ℓ_p . The corresponding real-space correlations extend to large length scales, as illustrated in Fig. 3(c). Such correlated velocity patterns have no equilibrium analog; they are a form of collective motion that emerges from the interplay of repulsive interactions and persistent motility in these liquids.

In addition, we use the velocity autocorrelation function $C_{vv}(t)$ to characterise fluctuations in time. Fig. 3(d) shows that these decay over a timescale that depends strongly on the persistence time τ_p (here $\tau_p = 1000 \gg 1$), and weakly on ϕ . Because particle motion is not strongly hindered by crowding in the active liquid, large particle displacements easily occur along the spatially correlated velocity field, which maintains its structure over long timescales $\sim \tau_p$. This is confirmed in Fig. 3(e) which shows that the MSD is superdiffusive for times up to τ_p , corresponding in real space to a spatially correlated displacement field [Fig. 3(f)] which resembles the velocity field at $t = 0$. The many vortices and abrupt changes of this velocity field, alongside its large-scale correlations, bear strong similarities with the family of active systems described as ‘turbulent’ [40–43] (see `SuppMovie1.mov` and `SuppMovie2.mov`): remarkably, this occurs here in an active liquid without explicit aligning interactions.

On increasing density, the system becomes crowded, and diffusive motion sets in over a large timescale $\tau_\alpha(\phi) \propto D^{-1}$ that increases rapidly with ϕ . At equilibrium, particle dynamics is triggered by infrequent thermally activated relaxation events characterised by a broad distribution of energy barriers, reflecting a rugged energy landscape [13]. This physical picture survives for modest values of the persistence times, as in Fig. 2(a), except that

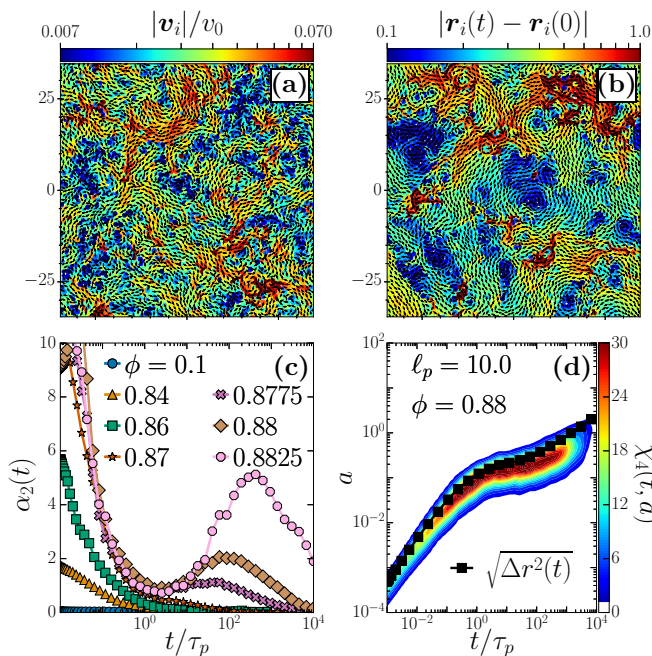


FIG. 4. (a) Velocity field for $N = 4096$, $\ell_p = 10$, $\phi = 0.8825$. (b) Displacement field after a time $t = 200\tau_p$ starting from the velocity field shown in (a) at $t = 0$. (c) Non-Gaussian parameter $\alpha_2(t)$ for $\ell_p = 10$, $N = 1024$ and different packing fractions. (d) Dynamical susceptibility $\chi_4(t, a)$ with $N = 1024$, $\ell_p = 10$, $\phi = 0.88$.

activated dynamics is now driven by a nonequilibrium colored noise, as recently studied in simpler active situations [44, 45]. Therefore, glassy dynamics for weak persistence qualitatively resembles passive systems [11, 18].

The physics is radically different when the persistence time is large, see Fig. 4. This opens a time window, $1 \ll t \ll \tau_p$, where particle dynamics is nearly arrested and $|\mathbf{v}_i| \ll |\mathbf{p}_i|$, see Fig. 2(b). This means that the forces stemming from particle interactions nearly balance the self-propulsion forces, and the system is close to a state of mechanical equilibrium. Such configurations correspond to local minima of an effective potential energy [46], $U_{\text{eff}}(\mathbf{r}; \mathbf{p}) \equiv U(\mathbf{r}) - \sum_i \mathbf{p}_i \cdot \mathbf{r}_i$, which depends on both positions and propulsions. Because U_{eff} evolves slowly (on a timescale $\tau_p \gg 1$), a mechanical equilibrium at time t may be unstable at time $t + \tau_p$, because the propulsion forces will have significantly evolved via Eq. (2). This loss of mechanical equilibrium triggers fast particle rearrangements [10] (on a timescale ~ 1), as the system relaxes towards a new minimum of U_{eff} .

This intermittent dynamics between mechanical equilibria superficially resembles plastic deformation in slowly sheared amorphous solids [47]. The separation of timescales means that the spatially correlated velocity field at $t = 0$ [see Fig. 4(a)] does not dictate particle displacements at larger times [Fig. 4(b)], in contrast to the persistent liquid [Figs. 3(c,f)]. Instead, the displace-

ment field results from the accumulation of particle rearrangements throughout the system. This still produces a spatially correlated displacement field [Fig. 4(b)], but its physical origin is then qualitatively distinct from both the turbulent flows seen in the persistent liquid and the activated relaxation events at weak persistence.

These qualitative observations about heterogeneous dynamics are confirmed using tools from equilibrium supercooled liquids [48]. Fig. 4(c) shows the non-Gaussian parameter

$$\alpha_2(t) = \frac{N^{-1} \sum_i \langle |\mathbf{r}_i(t) - \mathbf{r}_i(0)|^4 \rangle}{2(\Delta r^2(t))^2} - 1, \quad (4)$$

which is zero when the distribution of particle displacements is Gaussian, as in simple equilibrium fluids. In the persistent liquid ($\phi \lesssim 0.87$) then $\alpha_2(t)$ decreases monotonically with t , reflecting a smooth evolution from the non-Gaussian velocity distribution at $t = 0$ to the Gaussian diffusive limit at $t \gg \tau_p$. For the intermittent dynamics at large ϕ , $\alpha_2(t)$ starts off similar to the active liquid, but increases again for $t > \tau_p$. This is due to intermittent relaxations between minima of U_{eff} , which produce a maximum at a much longer timescale $\tau_\alpha \gg \tau_p$.

We also study the dynamic susceptibility [48]

$$\chi_4(t, a) = N [\langle Q^2(t, a) \rangle - \langle Q(t, a) \rangle^2], \quad (5)$$

where $Q(t, a) = \frac{1}{N} \sum \Theta(a - |\mathbf{r}_i(t) - \mathbf{r}_i(0)|)$ is a dynamic overlap and a a lengthscale, which probes the collective nature of the dynamics over a timescale t resolved over a lengthscale a . It is shown as a function of both these quantities in Fig. 4(d). In dense passive systems, $\chi_4(t, a)$ is only sizeable if $t \sim \tau_\alpha$ and a is of the order of the typical cage size, thus capturing the cooperative nature of activated relaxation. Here, $\chi_4(t, a)$ is large at all times, and is maximised for a given t for $a \sim \sqrt{\Delta r^2(t)}$. These data quantitatively confirm the visual impression from Figs. 4(a,b) that particle displacements are spatially correlated at both short and long time scales in very persistent glassy systems, in contrast to the passive case.

We end by surveying the collective motion that occurs in disordered active states. Weakly persistent systems display spatially heterogeneous dynamics near dynamic arrest, reminiscent of passive glasses. By contrast, strongly persistent systems support active liquid states with turbulent nonequilibrium flows and superdiffusive motion. At high density, the dynamic arrest of these liquids is accompanied by complex spatio-temporal correlations, spanning a range of length and time scales. It is remarkable that this rich phenomenology occurs in one of the simplest models of active particles without shapes, hydrodynamics or aligning interactions and is accessible by adjusting just two parameters in the unified setting of Fig. 1.

We thank L. Cugliandolo, J. Tailleur, and F. van Wijland for discussions. This work was supported by a grant from the Simons Foundation (#454935 L. Berthier).

-
- [1] M Cristina Marchetti, Jean-François Joanny, Sriram Ramaswamy, Tanniemola B Liverpool, Jacques Prost, Madan Rao, and R Aditi Simha, “Hydrodynamics of soft active matter,” *Reviews of Modern Physics* **85**, 1143 (2013).
- [2] Thomas E Angelini, Edouard Hannezo, Xavier Trepât, Manuel Marquez, Jeffrey J Fredberg, and David A Weitz, “Glass-like dynamics of collective cell migration,” *Proceedings of the National Academy of Sciences* **108**, 4714–4719 (2011).
- [3] Andrea Cavagna and Irene Giardina, “Bird flocks as condensed matter,” *Annual Review of Condensed Matter Physics* **5**, 183–207 (2014).
- [4] Nicolas Bain and Denis Bartolo, “Dynamic response and hydrodynamics of polarized crowds,” *Science* **363**, 46–49 (2019).
- [5] M. Rubenstein, A. Cornejo, and R. Nagpal, “Programmable self-assembly in a thousand-robot swarm,” *Science* **345**, 795–799 (2014).
- [6] Étienne Fodor and M. Cristina Marchetti, “The statistical physics of active matter: From self-catalytic colloids to living cells,” *Physica A: Statistical Mechanics and its Applications* **504**, 106–120 (2018).
- [7] Natsuda Klongvessa, Félix Ginot, Christophe Ybert, Cécile Cottin-Bizonne, and Mathieu Leocmach, “Active glass: Ergodicity breaking dramatically affects response to self-propulsion,” *Physical Review Letters* **123**, 248004 (2019).
- [8] Michael E Cates and Julien Tailleur, “Motility-induced phase separation,” *Annual Review of Condensed Matter Physics* **6**, 219–244 (2015).
- [9] Grzegorz Szamel and Elijah Flenner, “Long-ranged velocity correlations in dense systems of self-propelled particles,” *EPL (Europhysics Letters)* **133**, 60002 (2021).
- [10] Rituparno Mandal, Pranab Jyoti Bhuyan, Pinaki Chaudhuri, Chandan Dasgupta, and Madan Rao, “Extreme active matter at high densities,” *Nature Communications* **11**, 1–8 (2020).
- [11] Ludovic Berthier, Elijah Flenner, and Grzegorz Szamel, “Glassy dynamics in dense systems of active particles,” *The Journal of Chemical Physics* **150**, 200901 (2019).
- [12] Liesbeth MC Janssen, “Active glasses,” *Journal of Physics: Condensed Matter* **31**, 503002 (2019).
- [13] Ludovic Berthier and Giulio Biroli, “Theoretical perspective on the glass transition and amorphous materials,” *Reviews of Modern Physics* **83**, 587 (2011).
- [14] Ludovic Berthier and Jorge Kurchan, “Non-equilibrium glass transitions in driven and active matter,” *Nature Physics* **9**, 310–314 (2013).
- [15] Saroj Kumar Nandi, Rituparno Mandal, Pranab Jyoti Bhuyan, Chandan Dasgupta, Madan Rao, and Nir S. Gov, “A random first-order transition theory for an active glass,” *Proceedings of the National Academy of Sciences* **115**, 7688–7693 (2018).
- [16] Julian Reichert, Leon F Granz, and Thomas Voigtmann, “Transport coefficients in dense active brownian particle systems: mode-coupling theory and simulation results,” *The European Physical Journal E* **44**, 1–13 (2021).
- [17] Ludovic Berthier, “Nonequilibrium glassy dynamics of self-propelled hard disks,” *Physical Review Letters* **112**, 220602 (2014).
- [18] Elijah Flenner, Grzegorz Szamel, and Ludovic Berthier, “The nonequilibrium glassy dynamics of self-propelled particles,” *Soft Matter* **12**, 7136–7149 (2016).
- [19] Ludovic Berthier, Elijah Flenner, and Grzegorz Szamel, “How active forces influence nonequilibrium glass transitions,” *New Journal of Physics* **19**, 125006 (2017).
- [20] Natsuda Klongvessa, Félix Ginot, Christophe Ybert, Cécile Cottin-Bizonne, and Mathieu Leocmach, “Non-monotonic behavior in dense assemblies of active colloids,” *Physical Review E* **100**, 062603 (2019).
- [21] Qinyi Liao and Ning Xu, “Criticality of the zero-temperature jamming transition probed by self-propelled particles,” *Soft Matter* **14**, 853–860 (2018).
- [22] Peter K. Morse, Sudeshna Roy, Elisabeth Agoritsas, Ethan Stanifer, Eric I. Corwin, and M. Lisa Manning, “A direct link between active matter and sheared granular systems,” *Proceedings of the National Academy of Sciences* **118**, e2019909118 (2021).
- [23] Carlos Villarroel and Gustavo Düring, “Critical yielding rheology: from externally deformed glasses to active systems,” *arXiv preprint arXiv:2101.12345* (2021).
- [24] Silke Henkes, Kaja Kostanjevec, J Martin Collinson, Rastko Sknepnek, and Eric Bertin, “Dense active matter model of motion patterns in confluent cell monolayers,” *Nature Communications* **11**, 1–9 (2020).
- [25] Lorenzo Caprini and Umberto Marini Bettolo Marconi, “Active matter at high density: Velocity distribution and kinetic temperature,” *The Journal of Chemical Physics* **153**, 184901 (2020).
- [26] Gabriel S Redner, Michael F Hagan, and Aparna Baskaran, “Structure and dynamics of a phase-separating active colloidal fluid,” *Physical Review Letters* **110**, 055701 (2013).
- [27] Pasquale Digregorio, Demian Levis, Antonio Suma, Leticia F Cugliandolo, Giuseppe Gonnella, and Ignacio Pagonabarraga, “Full phase diagram of active brownian disks: From melting to motility-induced phase separation,” *Physical Review Letters* **121**, 098003 (2018).
- [28] Ahmad K. Omar, Katherine Klymko, Trevor GrandPre, and Phillip L. Geissler, “Phase diagram of active brownian spheres: Crystallization and the metastability of motility-induced phase separation,” *Physical Review Letters* **126**, 188002 (2021).
- [29] Yaouen Fily, Silke Henkes, and M Cristina Marchetti, “Freezing and phase separation of self-propelled disks,” *Soft Matter* **10**, 2132–2140 (2014).
- [30] Matteo Paoluzzi, Demian Levis, and Ignacio Pagonabarraga, “Are motility-induced phase-separation and glassiness compatible in dense active matter?” *arXiv preprint arXiv:2109.14948* (2021).
- [31] A. P. Solon, M. E. Cates, and J. Tailleur, “Active brownian particles and run-and-tumble particles: A comparative study,” *The European Physical Journal Special Topics* **224**, 1231–1262 (2015).
- [32] Grzegorz Szamel, “Self-propelled particle in an external potential: Existence of an effective temperature,” *Physical Review E* **90**, 012111 (2014).
- [33] N. Koumakis, C. Maggi, and R. Di Leonardo, “Directed transport of active particles over asymmetric energy barriers,” *Soft Matter* **10**, 5695–5701 (2014).
- [34] Claudio Maggi, Matteo Paoluzzi, Andrea Crisanti, Emanuela Zaccarelli, and Nicoletta Gnan, “Universality class of the motility-induced critical point in large scale off-lattice simulations of active particles,” *Soft Matter*

- 17, 3807–3812 (2021).
- [35] G. Briand and O. Dauchot, “Crystallization of Self-Propelled Hard Discs,” *Physical Review Letters* **117**, 098004 (2016).
- [36] G. Brambilla, D. El Masri, M. Pierno, L. Berthier, L. Cipelletti, G. Petekidis, and A. B. Schofield, “Probing the equilibrium dynamics of colloidal hard spheres above the mode-coupling glass transition,” *Physical Review Letters* **102**, 085703 (2009).
- [37] Umberto Marini Bettolo Marconi, Nicoletta Gnan, Matteo Paoluzzi, Claudio Maggi, and Roberto Di Leonardo, “Velocity distribution in active particles systems,” *Scientific Reports* **6**, 23297 (2016).
- [38] Grzegorz Szamel, Elijah Flenner, and Ludovic Berthier, “Glassy dynamics of athermal self-propelled particles: Computer simulations and a nonequilibrium microscopic theory,” *Physical Review E* **91**, 062304 (2015).
- [39] Andrea Cavagna, Irene Giardina, and Tomás S. Grigera, “The physics of flocking: Correlation as a compass from experiments to theory,” *Physics Reports* **728**, 1–62 (2018).
- [40] Henricus H. Wensink, Jörn Dunkel, Sebastian Heidenreich, Knut Drescher, Raymond E Goldstein, Hartmut Löwen, and Julia M Yeomans, “Meso-scale turbulence in living fluids,” *Proceedings of the National Academy of Sciences* **109**, 14308–14313 (2012).
- [41] Daiki Nishiguchi and Masaki Sano, “Mesoscopic turbulence and local order in janus particles self-propelling under an ac electric field,” *Physical Review E* **92**, 052309 (2015).
- [42] Amin Doostmohammadi, Tyler N Shendruk, Kristian Thijssen, and Julia M Yeomans, “Onset of meso-scale turbulence in active nematics,” *Nature Communications* **8**, 1–7 (2017).
- [43] Ricard Alert, Jaume Casademunt, and Jean-François Joanny, “Active Turbulence,” *Annual Review of Condensed Matter Physics* **13**, null (2022).
- [44] Eric Woillez, Yongfeng Zhao, Yariv Kafri, Vivien Lecomte, and Julien Tailleur, “Activated escape of a self-propelled particle from a metastable state,” *Physical Review Letters* **122**, 258001 (2019).
- [45] Eric Woillez, Yariv Kafri, and Nir S Gov, “Active trap model,” *Physical Review Letters* **124**, 118002 (2020).
- [46] Rituparno Mandal and Peter Sollich, “How to study a persistent active glassy system,” *Journal of Physics: Condensed Matter* **33**, 184001 (2021).
- [47] Craig E. Maloney and Anaël Lemaître, “Amorphous systems in athermal, quasistatic shear,” *Physical Review E* **74**, 016118 (2006).
- [48] Ludovic Berthier, Giulio Biroli, Jean-Philippe Bouchaud, Luca Cipelletti, and Wim van Saarloos, *Dynamical heterogeneities in glasses, colloids, and granular media*, Vol. 150 (OUP Oxford, 2011).

Supplementary movies

- **SuppMovie1.mov**: Fraction of a system of $N = 4096$ particles, at $\ell_p = 31.6$ and $\phi = 0.84$. Each frame are separated by a time $\delta t = 0.05\tau_p$ and the frame rate is 5fps.
- **SuppMovie2.mov**: Same system of $N = 4096$ particles, at $\ell_p = 31.6$ and $\phi = 0.84$. Particles are given a color (black or white) according to their position at $t = 0$ following a checkerboard pattern for better visualisation of the motion. Each frame are separated by a time $\delta t = 0.05\tau_p$ and the frame rate is 5fps.